Optics and Lasers in Engineering 136 (2020) 106310

Contents lists available at ScienceDirect

Optics and Lasers in Engineering

journal homepage: www.elsevier.com/locate/optlaseng

Single-shot color object reconstruction through scattering medium based on neural network

Enlai Guo, Yan Sun, Shuo Zhu, Dongliang Zheng, Chao Zuo, Lianfa Bai, Jing Han*

Jiangsu Key Laboratory of Spectral Imaging and Intelligent Sense, Nanjing University of Science and Technology, Nanjing 210094, China

ARTICLE INFO

Keywords:
Imaging through scattering medium
Single-shot speckle recovery
Color scattering imaging from broadband signal

ABSTRACT

The reconstruction of the color object hidden behind the scattering medium is very important because the human eye is much more sensitive to color than grayscale. Traditional methods are still difficult to reconstruct an accurate image of the hidden target from one single speckle image. In this paper, a single-shot color object reconstruction technique is proposed by designing a Color Anti-scattering Convolutional Neural Network (CASNet), which is trained to output the color and structure of the hidden color target from the input of a single speckle image. The proposed technique enables us to reconstruct the target with accurate color and structure from a broadband speckle image, and the average PSNR of recovered targets with complex structure is higher than 24dB. Efficiency and accurateness are verified through experiments.

1. Introduction

The image recovery of object hidden behind scattering media is important for biomedicine, degraded environment imaging and astronomical imaging [1], etc. Traditional methods recover the object from several (multi-shot) speckle images or a single (i.e., single-shot) speckle image [2–11]. The multiple-shot can recover the accurate object whose corresponding speckle images are in a broadband spectrum [11,12], but it is not suitable for dynamic scattering media due to its time consuming. The single-shot can be used for dynamic scattering media due to its high data acquisition speed, but it can only recover the accurate object whose corresponding speckle image is in a narrow spectrum (i.e., less than 20*nm*) [2,3]. Therefore, an additional reference source has been used for single-shot grayscale object recovery using a broadband speckle image [8].

As we know, the contrast of speckle images is inverse-proportional to the spectrum bandwidth of the light signal, and a low-contrast speckle image reduces the recovery accuracy [2,3]. However, the low-contrast speckle image is inevitable for color object recovery, because the spectrum of color object is in a wide range (i.e., ranges from 380*nm* to 780*nm*). To alleviate the influence of the low speckle contrast, traditional single-shot color object recovery methods are assisted with the feedback signal, system property or additional hardware [13–17]. The feedback signal-assisted method requires a reference source in each measurement [13], which is inconvenience in real application. The system property-assisted method requires an absolutely stable optical system [12,14–16], which cannot be used for dynamic scattering media. The hardware-assisted method requires additional prism and coding template [17], which has a limited field of view (FOV) due to the constraint of the optical memory effect (i.e., OME).

In addition, the recovered targets are relatively simple objects [2–23], such as characters, simple graphics, or images with strong structural consistency, etc. Traditional physical model-based methods are still difficult to recover complex color objects containing rich structural details, such as texture and color varieties. As aforementioned, most traditional single-shot color object recovery methods are inconvenience, inaccurate or target-limited, because the color object recovery requires to obtain the structure and spectrum simultaneously. Deep learning-based recovery methods perform better than traditional physical model-based recovery in accuracy and efficiency [18–23], which show great potential in single-shot color object recovery.

In this paper, a color anti-scattering convolutional neural network (i.e., CASNet) is constructed, that maps a single low-contrast speckle image to the hidden color target. Designed based on the separability of spectral dimension in the scattering process, CASNet has good target structure recovery ability and high computational efficiency. A series of real objects in the life scene are recovered with at least twice of the OME range, and the average Structural Similarity Index (SSIM) of recovered images is larger than 0.86.

The rest of the paper is organized as follows. Section 2 illustrates the principle of CASNet. Section 3 gives experiments. Section 4 concludes this paper.

* Corresponding author
E-mail addresses: dlzheng@njust.edu.cn (D. Zheng), mrblf@njust.edu.cn (L. Bai), eohj@njust.edu.cn (J. Han).

https://doi.org/10.1016/j.optlaseng.2020.106310
Received 25 March 2020; Received in revised form 22 June 2020; Accepted 16 July 2020
Available online xxx

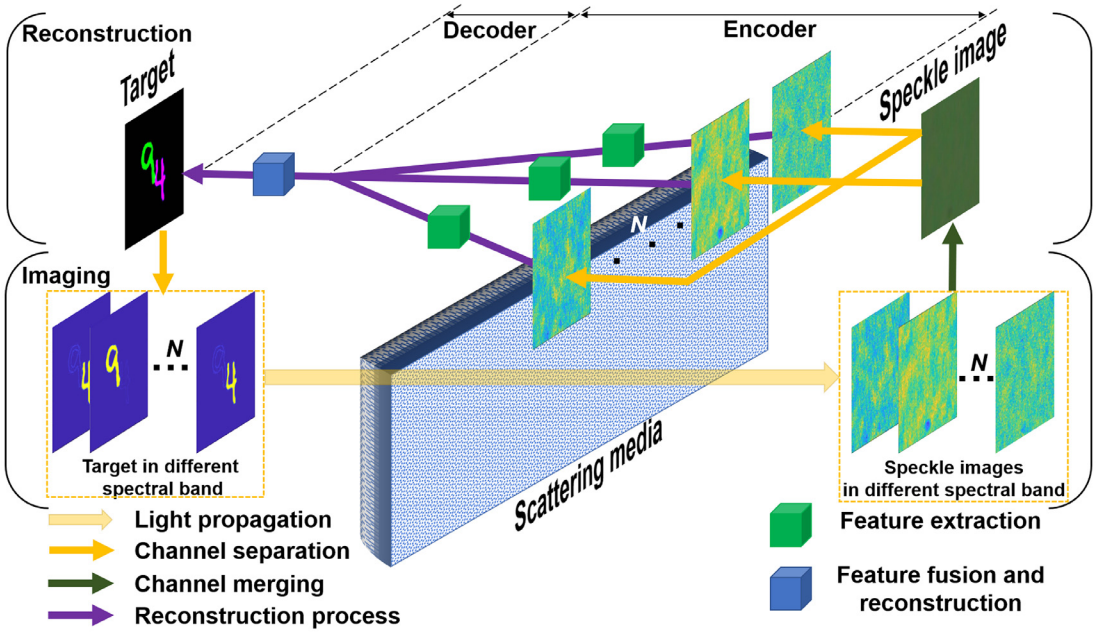

Fig. 1. The Color target imaging and recovery process.

2. Principle

The schematic diagram of the imaging and recovering through scattering media is illustrated in Fig. 1. In the imaging process, the captured speckle image of the target is the composition of sub-speckle images, which are formed by imaging the original target in different bands through the scattering media. The number of spectral bands is denoted by N, which equals to 3 (i.e., red, green, and blue) for the color target imaging. In the recovery process, an encoder with three independent network structures are employed to extract features of red, green, and blue speckle channels, because multi-channel speckle images are physically separable [16,17]. A subsequent decoder is used to fuse the extracted higher-level features and restore the structure and color of the original target. The theoretical analysis and the neural network design are detailed as follows.

A. Theoretical analysis

On the one hand, speckle images of the objective target outside the OME range can be regarded as the composition of sub-speckles generated by sub-targets within the OME range. On the other hand, the speckle image of each sub-target is composed of speckle images with different spectral bands. The number of sub-targets is denoted by M, and the resulting speckle image can be expressed as

$$I_{MN} = \sum_{n=1}^{N}\sum_{m=1}^{M} O_{t_m\lambda_n} * PSF_{t_m\lambda_n}, \tag{1}$$

where $*$ denotes the convolution operation, λ_n represents the n-th spectral band, O_{t_m} is the intensity of m-th sub-target of the objective target, and $PSF_{t_m\lambda_n}$ is the system PSF of the imaging region of the m-th sub-target in n-th spectral band. According to Eq. (1), both the spatial information and the spectral information contribute to the speckle image of the target, which would lower the contrast of broadband speckle image [2]. Considering the scattering process of the target outside the range of OME formed by a single spectral band λ_1, the captured speckle image becomes [24–26]

$$I_{M1} = \sum_{m=1}^{M} O_{t_m} * PSF_{t_m}. \tag{2}$$

Considering a small target in the OME region and illuminated by a broadband light source, the captured speckle image is [16,17]

$$I_{1N} = \sum_{n=1}^{N} O_{\lambda_n} * PSF_{\lambda_n}. \tag{3}$$

Deep learning has been successfully introduced to recover the hidden gray objects beyond OME [18–23], e.g., recovering O_{λ_1} from I_{M1}, according to Eq. (2). Because Eq. (3) has the same form as Eq. (2), deep learning can also recover a small target (i.e., in the OME range) illuminated by a broadband light. The problem of the single-shot color object recovery described by Eq. (1), requires to recover the structure of the object beyond the OME range (i.e., the problem described by Eq. (2)) and restore the color information with a broadband (i.e., the problem described by Eq. (3)). Therefore, deep learning provides a feasible way for the single-shot color object recovery through the following reasonable network structure design.

B. The neural network design

In order to recover the structure and the color of the target from a single frame broadband speckle image, CASNet is designed with the Encoder-Decoder structure, as shown in Fig. 2. The Encoder is designed to extract features from the captured speckle image, and the Decoder is used to recover the hidden target from these extracted features. The speckle image captured by the camera is selected as the input of CASNet. The desired color image of the target is selected as the ground truth (i.e., GT) of CASNet, which is the image in the same scene without scattering medium. The similarity between the recovered image and the ground-truth image is evaluated by a loss function and used to optimize network parameters.

Before the feature extraction, we emphasize that most color feature extraction methods for non-scattering tasks usually take the three channels as a whole due to the structural correlation among the three channels [27–29]. However, the light signal containing original target information is scattered by the scattered medium and becomes a seemingly disordered speckle image, which greatly weakens the original structural correlation between different bands. The spectral bandwidth of all the three sub-speckle images is above 100nm, which exceeds the decorrelation bandwidth of the scattering medium, and results in the irrelevance between the three sub-speckle images. If the Encoder is only composed of a single network unit with a single input of the whole speckle image,

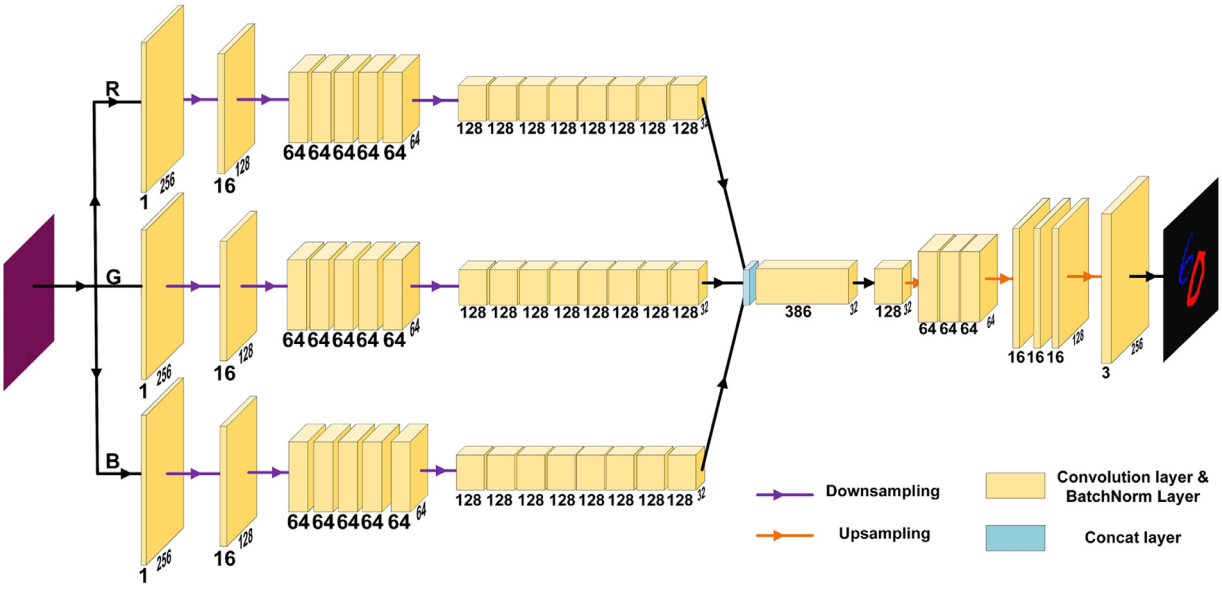

Fig. 2. The network structure diagram of CASNet.

it is difficult to extract accurate features to represent the structure of the target in different channels due to the irrelevance of the sub-speckle images.

Therefore, the Encoder of CASNet uses three network units independently to extract features for the color target recovery. The speckle image of the color target is divided into three sub-speckle images (i.e., red, green, and blue channels). The Encoder is composed of three branches with the same structure, which are employed to extract high-level features from the three speckle images, respectively. Together with some convolutional layers, the Concat layer merges these extracted features into one matrix, which is sent into the Decoder to recover the structure-color information of the target. Because the red, green and blue channels of the target, namely GT, are structurally correlated, the Decoder uses a single-branch structure to fully use the correlation among the three channels. The input of CASNet is an 8-bit speckle image with a resolution of 256*256, and the output is a three-channel image with a size of 256*256. The depthwise separable convolution is used to improve the efficiency and promise the accuracy. The dilated convolution is used to extract features under different sizes of receptive fields. The dropout strategy is used to avoid over-fitting during training. In the training process, mean square error (MSE) is used as the main loss function, and SSIM is employed to guide the direction of network optimization by constraining the overall structure of the recovered result. The network loss function can be expressed as

$$Loss = MSE + w * (1 - SSIM), \tag{4}$$

where w is the weight factor used to balance MSE and SSIM.

3. Experiments

The experiments use a lens-free optical system as shown in Fig. 3(a), which includes a LED projector (Robot GO M6S, 1280*720 DPI), a ground glass (Thorlabs, DG100X100-220, 220 grit), an iris (Thorlabs, ID25SS/M, maximum aperture 25*mm*, diameter 8*mm*), and an industrial camera (Basler acA1920-40gc, 1920*1200 pixels, 5.86μm). The targets are generated by a computer and then projected by the projector, which reach the camera image sensor through the ground glass. The camera captures the speckle image with a spectral bandwidth of over 300*nm*. The size of the speckle is adjusted by the iris behind the ground glass. The distance between the projector and the ground glass is 100*cm* according to the shortest projection distance of the projector, and the distance between the ground glass and the camera is 10*cm*. The spectral curve of the projector is measured by a spectrometer (Ocean Optics USB2000+), and its spectral bandwidth is shown in Fig. 3(b). The infrared cut-off filter in front of the camera sensor prevents the part of the projector's optical signal from reaching the camera, which has a spectrum range of 700*nm*-750*nm*. In order to make all the scattered signals reach the camera, the cut-off filter of the camera is removed before the experiment. The designed CASNet is trained and tested on PyTorch 1.2.0 with RTX 2080Ti and i7-9700k CPU under ubuntu 16.04.

The performance of CASNet is evaluated by analyzing the structure and the color difference between the recovered image and the ground-truth image. The structure difference is described by the Mean Absolute Error (MAE), SSIM and Peak Signal to Noise Ratio (PSNR). The color difference is defined as the average value of CIEDE2000, and can be calculated by [30,31]

$$\Delta E_{00} = \sqrt{(\frac{\Delta L'}{k_L S_L})^2 + (\frac{\Delta C'}{k_C S_C})^2 + (\frac{\Delta H'}{k_H S_H})^2 + R_T(\frac{\Delta C'}{k_C S_C})(\frac{\Delta H'}{k_H S_H})}, \tag{5}$$

where $\Delta L'$, $\Delta C'$ and $\Delta H'$ are respective the lightness difference, the chroma difference and the hue difference; k_L, k_C and k_H are parameter factors that are used for correction coefficients; S_L, S_C and S_H are the weight parameters that are used to correct the uniformity of color space; R_T is the rotation term that is used to correct the deflection of the principal axis of the ellipse in the blue region of the color space.

To demonstrate the designed CASNet, the following experiments include recovering gray target from a broadband speckle image, simple color target of characters, complex color target in real scenes, and color target with large different features.

A. Experiment on grayscale target recovery from a wide spectral speckle image

A ***wide-spectrum gray-double-character dataset*** (i.e., ***WGC***) is constructed, where each data pair includes a grayscale target (i.e., the ground truth) and its corresponding broadband speckle image (i.e., the corresponding input). The ground-truth target is generated by the random combination of handwritten characters selected from MINIST [32], which is projected onto the scattering medium by the projector. The resulting broadband speckle image is captured by the camera. Because the captured image is a single-channel grayscale speckle image, a three-channel speckle image is formed as the input of CASNet by copying the single channel to other two channels. The output of CASNet is a single channel image by changing the output dimension of the last layer to

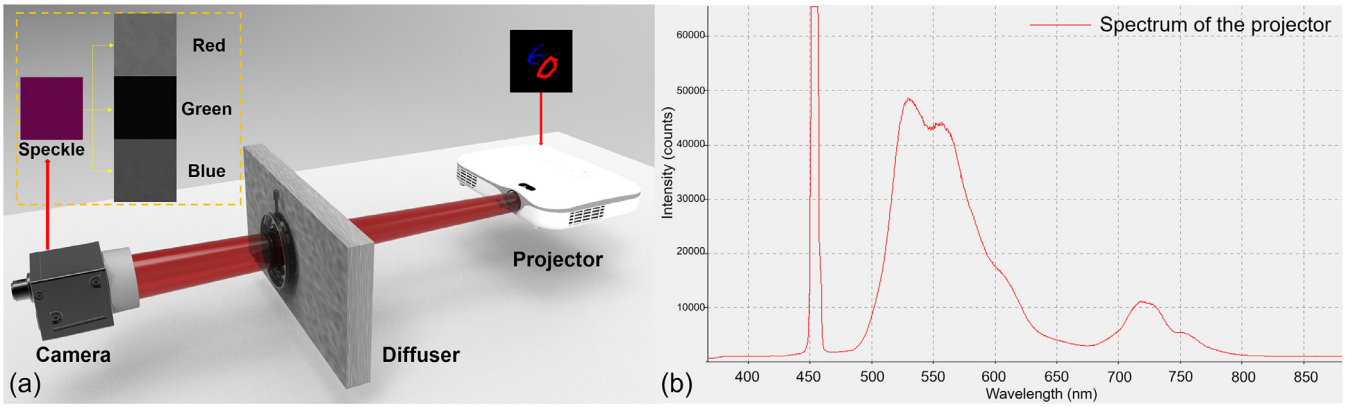

Fig. 3. The structure of the optical system: (a) optical setup; (b) the spectrum of the projector measured by spectrometer (Ocean Optics USB2000 +).

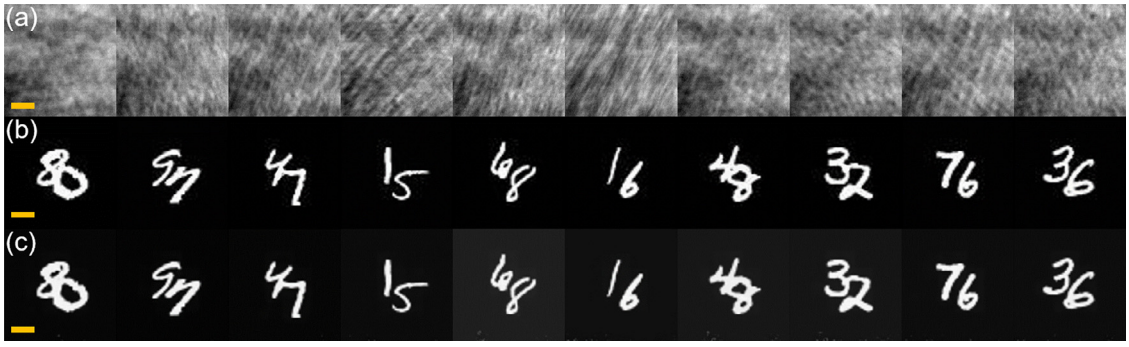

Fig. 4. The recovered results of the untrained gray targets from broadband light signals by CASNet: (a) the gray speckle image with wide spectrum; (b) GT of (a); (c) the recovered result from (a). Scale bars: 50 pixels.

Table 1
The average MAE, SSIM, PANR and value of CIEDE2000 of the testing sets.

The untrained testing set	MAE	SSIM	PSNR	CIEDE2000
The ***WGC*** dataset	1.6893	0.9517	33.9866	———
The ***CDC*** dataset	1.8287	0.9609	25.4485	1.0144
The ***CCT*** dataset	5.6942	0.8654	24.7228	2.7146

256*256*1 according to Fig. 2. The constructed dataset contains 8000 targets, where 7500 and 500 targets are used for the training and the testing, respectively. It should be noted that all the testing targets are not used in the training.

The experimental results of the testing set are shown in Fig. 4. The resulting speckle images have the low contrast due to the broadband lighting as shown in Fig. 4(a), which are used to recover the corresponding hidden targets. The recovered targets shown in Fig. 4(c) are well consistent with the ground-truth targets as shown in Fig. 4(b). The overall structure and local detail are accurate. The average PSNR and SSIM of recovered images are respective 33.98dB and 0.9517 as provided in Table 1.

B. Experiment on the color characters recovery

A ***color-double-character dataset*** (i.e., ***CDC***) is constructed, where each data pair includes a color target and its corresponding three-channel speckle image. The color target is generated by randomly coloring two characters selected from MINST [32], and the corresponding three-channel speckle images are captured as the input. Similarly, the random 7500 GT-input data pairs are taken as the training set and the other 500 groups as the testing set.

The recovered results of the testing targets are shown in Fig. 5, where Fig. 5(a)-5(c) are the speckle images, the ground-truths, and the recovered results, respectively. Although the contrast of the speckle decreases significantly due to the broadband lighting, both the structure and the color of the target are accurately recovered. The average PSNR of the restored images is 25.4485dB, which is slightly lower than that of the grayscale target because the recovery of the color target is more complex than that of the grayscale target. The recovered color target only contains a small part of discontinuous structure and color deviation for some special cases. For example, the upper half of the number *6* in the recovered image is structurally discontinuous in the fourth column of Fig. 5 and the partial edge of the number *4* is incorrectly recovered as blue in the last column in Fig. 5.

C. Experiment on the complex color objects recovery

The commonly used characters, simple graphics and structural surface are relatively simple scene [2–23]. It is still difficult to recover hidden targets for complex real scenes. A ***complex color target dataset*** (i.e., ***CCT***) is constructed, which contains the target in the ALOI dataset as the ground-truth [33,34]. These complex targets have more complicated structure and color than the handwritten characters. The corresponding speckle images are constructed as the input. The number of data pairs in the training set is increased to 23,649 pairs due to the complex structure. The testing set contains 848 data pairs without training. It should be noted that the objects in the testing set never appear in the training set. The experimental results of the testing set are shown in Fig. 6. Fig. 6(a) shows the speckle image of the three channels, Fig. 6(b) shows the ground-truth, and Fig. 6(c) shows the recovered image.

Most structure and color of the target are recovered. Unlike previous experiments with two-character targets, blurred edges appear in the recovered results for these complex targets. The blur phenomenon is mainly caused by the rich details of the targets, the low contrast of the speckle image, the abundant types of target, and the inconsistent size of the targets, etc. Compared with the results of the previous two experiments, the average MAE of the recovered images increases to 5.6942,

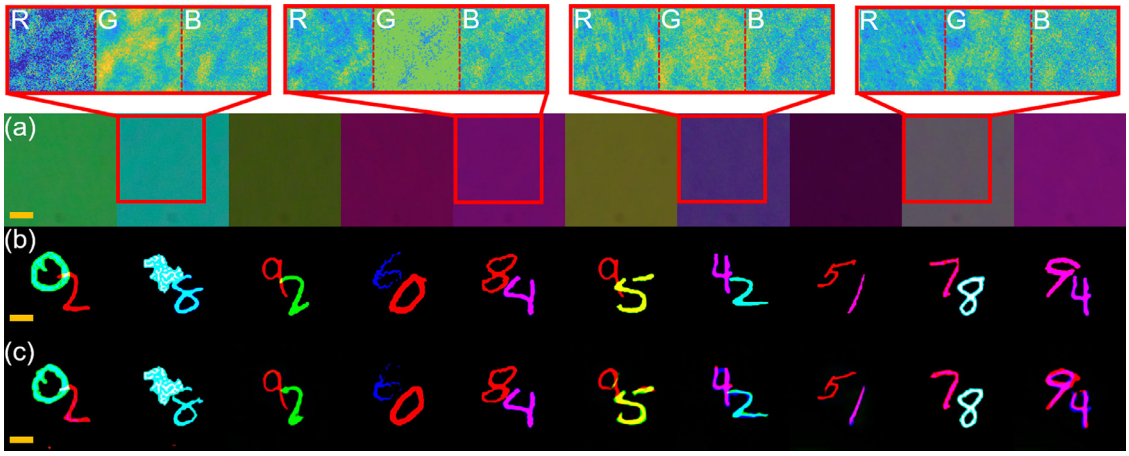

Fig. 5. The recovered results of the untrained color targets with two characters: (a) color speckle image, and the images above (a) are the red, green and blue channels of the speckle image; (b) GT of (a); (c) the recovered result from (a). Scale bars: 50 pixels. (For interpretation of the references to colour in this figure legend, the reader is referred to the web version of this article.)

Fig. 6. The recovered results of the testing set of the ***CCT*** dataset: (a) color speckle image; (b) GT of (a); (c) the recovered results from(a). Scale bars: 50 pixels.

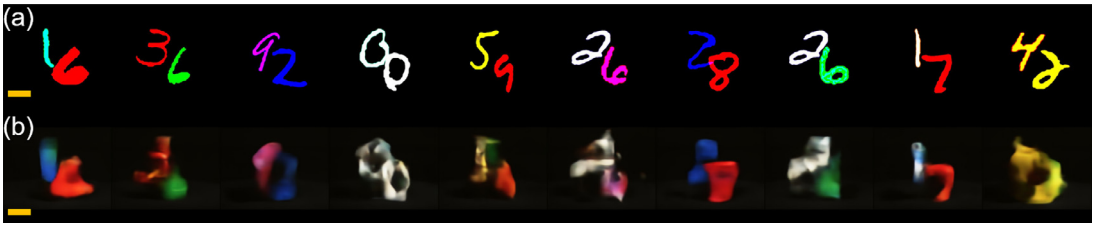

Fig. 7. The testing results of the ***CDC*** dataset recovered by the model trained with targets of ALOI: (a) GT; (b) the recovered results. Scale bars:50 pixels.

while the average SSIM decreases to 0.8654 and the average value of CIEDE2000 increases from 1.0144 to 2.7146, as shown in the Table 1. Consistent with the experimental conclusion in Ref. 23, similar experimental results are obtained by recovering the targets from the speckle images, which are collected through four scattering media with the same optical properties.

D. Experimental analysis of network's requirement for feature similarity and recovery speed

It should be emphasized that the training set and the testing set are required to have consistent features, because deep learning relies on known data to learn the relationship between the input and the output. Therefore, it is difficult to recover accurate color target with inconsistent features. For example, ***CCT*** trained CASNet is tested on ***CDC***. The testing results are shown in Fig. 7, where Fig. 7(a) and 7(b) are the ground-truths and the recovered results, respectively.

As shown in Fig. 7(b), there is a heavy blur of the recovered targets due to the large difference in the features of targets between the training set and the test set. The trained model needs to solve the unknown line-like structure from the known mapping relation, which greatly increases the difficulty of the double-color-characters recovery. For example, the line-like structure of the numbers *1* and *6* in the first example in Fig. 7 is almost absent from the complex targets in the training set.

The training set of the ***CCT*** dataset is used to test the recovering speed of CASNet, and the results show that the average Frames Per Second (FPS) of CASNet is up to 45. The timeliness of CASNet is good enough to meet the requirements of real-time recovery.

E. Discussion

According the experimental results, we have the following discussions.

(i) CASNet is able to reconstruct hidden targets from a single frame of broadband speckle image, which has been proved by experiments on multiple targets such as gray double characters, color double characters and complex targets in ALOI.

(ii) CASNet can still reconstruct the overall structure and approximate colors with blur edges, even for the complex targets in the experiment of the ***CCT*** dataset. As the complexity of the recovered target increases, the consistency of the structure-color information between the recovered image and the ground-truth of the hidden target declines.

(iii) CASNet needs similar feature information of targets in the training set and testing set to realize recovery due to the dependence of learning-based methods on data, otherwise it will lead to a significant decline in the quality of the recovered images. Meanwhile, it should be noted that the learning-based approach can still build mapping relationships that are not relevant to the scenario, and the premise is that the amount of data contained in the training set needs to be sufficient for the algorithm to learn all the features and details.

(iv) It should be noted that, the complex target recovered by CASNet appears the phenomenon of edge blurring, due to the large amount of target details contained in the low-contrast speckle image and the limited sensitivity of the industrial camera. On the other hand, the variable target size and object type further increases the difficulty of accurately recovering the target edge. This is also difficult to solve for the existing traditional algorithms.

4. Conclusion

In this paper, deep learning is introduced to recover the hidden color target, which enables a single-shot complex color object recovery under true broadband illumination. This breakthrough, recovering the color target with rich details from a single-shot speckle image possible, is an important step to eliminate the interference of the scattering media, and also provides an opportunity for imaging through dynamic scattering media.

Declaration of Competing Interest

The authors declare that they have no known competing financial interests or personal relationships that could have appeared to influence the work reported in this paper.

CRediT authorship contribution statement

Enlai Guo: Methodology, Validation, Writing - original draft. **Yan Sun:** Investigation, Data curation. **Shuo Zhu:** Software. **Dongliang Zheng:** Writing - review & editing. **Chao Zuo:** Writing - review & editing, Formal analysis. **Lianfa Bai:** Supervision, Funding acquisition. **Jing Han:** Conceptualization, Writing - review & editing, Project administration, Funding acquisition.

Acknowledgments

This research is supported by the Natural Science Foundations of China (61727802 and 61971227); The Key Research and Development programs in Jiangsu China (BE2018126). And we thank Xiaotian Lou, Yingjie Shi, Jie Gu and Qianying Cui for technical supports.

Supplementary material

Supplementary material associated with this article can be found, in the online version, at 10.1016/j.optlaseng.2020.106310

References

[1] Goodman JW. Speckle phenomena in optics: theory and applications. Roberts and Company Publishers; 2007.
[2] Katz O, Heidmann P, Fink M, Gigan S. Non-invasive single-shot imaging through scattering layers and around corners via speckle correlations. Nat Photonics 2014;8(10):784.
[3] Li H, Wu T, Liu J, Gong C, Shao X. Simulation and experimental verification for imaging of gray-scale objects through scattering layers. Appl Opt 2016;55(34):9731–7.
[4] Shi Y, Liu Y, Wang J, Wu T. Non-invasive depth-resolved imaging through scattering layers via speckle correlations and parallax. Appl Phys Lett 2017;110(23):231101.
[5] Wang Z, Jin X, Dai Q. Non-invasive imaging through strongly scattering media based on speckle pattern estimation and deconvolution. Sci Rep 2018;8(1):1–11.
[6] Li X, Stevens A, Greenberg JA, Gehm ME. Single-shot memory-effect video. Sci Rep 2018;8(1):1–8.
[7] Guo C, Liu J, Wu T, Zhu L, Shao X. Tracking moving targets behind a scattering medium via speckle correlation. Appl Opt 2018;57(4):905–13.
[8] Xu X, Xie X, Thendiyammal A, Zhuang H, Xie J, Liu Y, et al. Imaging of objects through a thin scattering layer using a spectrally and spatially separated reference. Opt Express 2018;26(12):15073–83.
[9] Okamoto Y, Horisaki R, Tanida J. Noninvasive three-dimensional imaging through scattering media by three-dimensional speckle correlation. Opt Lett 2019;44(10):2526–9.
[10] Lu D, Liao M, He W, Pedrini G, Osten W, Peng X. Tracking moving object beyond the optical memory effect. Opt Lasers Eng 2020;124:105815.
[11] Li L, Li Q, Sun S, Lin H-Z, Liu W-T, Chen P-X. Imaging through scattering layers exceeding memory effect range with spatial-correlation-achieved point-spread-function. Opt Lett 2018;43(8):1670–3.
[12] Zhu L, Wu Y, Liu J, Wu T, Liu L, Shao X. Color imaging through scattering media based on phase retrieval with triple correlation. Opt Lasers Eng 2020;124:105796.
[13] Conkey DB, Piestun R. Color image projection through a strongly scattering wall. Opt Express 2012;20(25):27312–18.
[14] Zhuang H, He H, Xie X, Zhou J. High speed color imaging through scattering media with a large field of view. Sci Rep 2016;6:32696.
[15] French R, Gigan S, Muskens OL. Speckle-based hyperspectral imaging combining multiple scattering and compressive sensing in nanowire mats. Opt Lett 2017;42(9):1820–3.
[16] Sahoo SK, Tang D, Dang C. Single-shot multispectral imaging with a monochromatic camera. Optica 2017;4(10):1209–13.
[17] Li X, Greenberg JA, Gehm ME. Single-shot multispectral imaging through a thin scatterer. Optica 2019;6(7):864–71.
[18] Li S, Deng M, Lee J, Sinha A, Barbastathis G. Imaging through glass diffusers using densely connected convolutional networks. Optica 2018;5(7):803–13.
[19] Li Y, Xue Y, Tian L. Deep speckle correlation: a deep learning approach toward scalable imaging through scattering media. Optica 2018;5(10):1181–90.
[20] Yang M, Liu Z-H, Cheng Z-D, Xu J-S, Li C-F, Guo G-C. Deep hybrid scattering image learning. J Phys D 2019;52(11):115105.
[21] Sun Y, Shi J, Sun L, Fan J, Zeng G. Image reconstruction through dynamic scattering media based on deep learning. Opt Express 2019;27(11):16032–46.
[22] Lyu M, Wang H, Li G, Zheng S, Situ G. Learning-based lensless imaging through optically thick scattering media. Adv Photonic 2019;1(3):036002.
[23] Guo E, Zhu S, Sun Y, Bai L, Zuo C, Han J. Learning-based method to reconstruct complex targets through scattering medium beyond the memory effect. Opt Express 2020;28(2):2433–46.
[24] Guo C, Liu J, Li W, Wu T, Zhu L, Wang J, et al. Imaging through scattering layers exceeding memory effect range by exploiting prior information. Opt Commun 2019;434:203–8.
[25] Wang X, Jin X, Li J, Lian X, Ji X, Dai Q. Prior-information-free single-shot scattering imaging beyond the memory effect. Opt Lett 2019;44(6):1423–6.
[26] Wang X, Jin X, Li J. Blind position detection for large field-of-view scattering imaging. Photonics Res 2020;8(6):920–8.
[27] Dong W, Wang P, Yin W, Shi G, Wu F, Lu X. Denoising prior driven deep neural network for image restoration. IEEE Trans Pattern Anal Mach Intell 2018;41(10):2305–18.
[28] Dai T, Cai J, Zhang Y, Xia S-T, Zhang L. Second-order attention network for single image super-resolution. In: Proceedings of the IEEE conference on computer vision and pattern recognition; 2019. p. 11065–74.
[29] Zhao H, Shao W, Bao B, Li H. A simple and robust deep convolutional approach to blind image denoising. In: Proceedings of the IEEE International Conference on Computer Vision Workshops; 2019. 0–0
[30] Luo MR, Cui G, Rigg B. The development of the cie 2000 colour-difference formula: ciede2000. Color Research & Application: Endorsed by Inter-Society Color Council, The Colour Group (Great Britain), Canadian Society for Color, Color Science Association of Japan, Dutch Society for the Study of Color, The Swedish Colour Centre Foundation, Colour Society of Australia, Centre Français de la Couleur 2001;26(5):340–50.
[31] Sharma G, Wu W, Dalal EN. The ciede2000 color-difference formula: implementation notes, supplementary test data, and mathematical observations. Color Research & Application: Endorsed by Inter-Society Color Council, The Colour Group (Great Britain), Canadian Society for Color, Color Science Association of Japan, Dutch Society for the Study of Color, The Swedish Colour Centre Foundation, Colour Society of Australia, Centre Français de la Couleur 2005;30(1):21–30.
[32] Yann LeCun, Corinna Cortes, Christopher J.C. Burges. THE MNIST DATABASE of handwritten digits. http://yann.lecun.com/exdb/mnist/;
[33] Jan-Mark Geusebroek, Gertjan J. Burghouts, Arnold W.M. Smeulders. Amsterdam Library of Object Images (ALOI). http://aloi.science.uva.nl/;
[34] Geusebroek J-M, Burghouts GJ, Smeulders AW. The amsterdam library of object images. Int J Comput Vis 2005;61(1):103–12.